Plasma-catalytic ammonia synthesis over $BaTiO_3$ supported metal catalysts: Process optimization using response surface methodology

Jin Liu[1], Xinbo Zhu[1, *], Chunlin Zhou[1], Jiali Du[1], Yuting Gan[1], Geng Chen[1], Xin Tu[2, *]

[1] Faculty of Maritime and Transportation, Ningbo University, Ningbo 315211, P.R. China

[2] Department of Electrical Engineering and Electronics, University of Liverpool, Liverpool L69 3GJ, United Kingdom

Abstract: Non-thermal plasma (NTP) assisted ammonia (NH_3) synthesis has been performed in a packed-bed dielectric barrier discharge (DBD) reactor. The presence of M/$BaTiO_3$ (M = Fe, Co and Ni) catalysts in the DBD reactor significantly improved the NH_3 concentration and energy efficiency with a sequence of Ni/$BaTiO_3$ > Co/$BaTiO_3$ > Fe/$BaTiO_3$ > $BaTiO_3$. N_2 adsorption-desorption experiment, X-ray diffraction analysis and temperature-programmed desorption of CO_2 were performed to get insight into the relationships between the plasma-assisted NH_3 synthesis process and M/$BaTiO_3$ catalysts. The improved performance over Ni/$BaTiO_3$ could be attributed to abundant basic sites and weaker metal-nitrogen (M-N) bindings on catalyst surfaces, which benefits the generation of NH_x species and desorption of formed NH_3. Response surface methodology (RSM) was utilized to assess the contribution of each independent process parameters and explore the mutual effects on NH_3 synthesis process systematically. The results of analysis of variance (AVONA) suggested that plasma discharge power and gas flow rate were the most significant factors in affecting the NH_3 concentration and energy efficiency of plasma-assisted NH_3 synthesis process, respectively. Based on the proposed polynomial regression model, the maximum energy efficiency of 2.37 g kWh^{-1} was achieved at the predicted optimal working condition over Ni/$BaTiO_3$.

Keywords: Plasma; Ammonia synthesis; M/$BaTiO_3$; DoE; RSM

1 Introduction

Ammonia (NH_3) has been widely used as the nitrogen source for fertilizer for hundreds of years. Recently, NH_3 presents a great potential to be considered as a carbonless fuel since the greenhouse gas emissions could be reduced by over 30% for ammonia-driven vehicles compared to those of gasoline- or diesel-driven vehicles [1]. Currently, the industrial-scale NH_3 synthesis method is Haber-Bosch (HB) method, which requires several harsh working conditions, e.g. sustained high temperature (500–600 °C) and high pressure (20–40 MPa). Due to the high energy consumption, great efforts have been devoted to develop greener and more sustainable alternatives for NH_3 synthesis, including biochemical and electrochemical processes, etc [2, 3]. Among these methods, NH_3 synthesis using non-thermal plasma (NTP) based technology has attracted extensive attention since this technology can be driven by renewable energy sources such as wind and solar power. Moreover, the plasma-assisted NH_3 synthesis process could be started and stopped very quickly by activating and deactivating the plasma, and be conducted under ambient conditions on a small-scale to realize the decentralized NH_3 production. To achieve NH_3 synthesis in a continuous fashion and hence improve the energy efficiency of the process, the studies published in recent years mainly focused on the synthesis of NH_3 using dielectric barrier discharge (DBD) plasma [4].

In the packed-bed DBD system, the optimization of process parameters is the fundamental to improve the performance of NH_3 synthesis. since the process parameters are directly related to electrical characteristics of plasma and could further affect electron-impact reactions, namely the initial step of plasma chemistry. Many previous works reported the effects of individual process

parameters on NH_3 synthesis [5–8]. However, these works were inadequate to optimize the plasma-assisted NH_3 synthesis process due to the lack of consideration on the mutual effects of process parameters. Recently, response surface methodology (RSM) has been used to study with a specific focus on the interactions between input parameters and on the optimization of the process for various complex processes. RSM is a statistical model considering the non-linear relationships between the multiple input and output variables. Based on the design of experiments (DoE), RSM could demonstrate the interactions among various process variables and determine the optimum conditions on the multiple responses [9]. RSM has been widely used in various chemical processes to optimize the process parameters, such as methane dry reforming [10], VOCs oxidation [11, 12] and NO_x removal [13]. However, to the best of our knowledge, the application of RSM in the optimization of plasma-assisted NH_3 synthesis process has not been investigated.

Catalysts are also of great significance in the plasma-catalysis system. The presence of heterogeneous catalyst in the plasma region could generate a synergistic effect, achieving better catalytic performance than the sum of performance achieved using plasma and heterogeneous catalyst individually. The synergistic effect could be attributed to both the enhancement of plasma discharge and the interactions between the active species and catalysts [14–16]. Currently, Ru based catalysts are regarded as the second-generation highly effective catalysts for NH_3 synthesis via HB method. However, the industrial-scale application of Ru based catalysts is hindered due to the high price and scarcity of Ru metal. Since the vibrational excited species generated in plasma could break the thermal dynamic limitations in conventional thermal catalytic process, the optimal active metal are predicted to be metals that bind nitrogen more weakly (e.g. Co or Ni) compared with Ru [17]. Hence, these transition metals have attracted wide attention and expected to be ideal substitutes for

conventional noble metal for plasma-assisted NH_3 synthesis to obtain optimum catalytic activity and better economic performance. On the other hand, barium titanate ($BaTiO_3$) is a typical ferroelectric material with a wide range of application in thermal and photo catalysis due to its high oxygen storage capacity and basic sites [18–20]. Our previous work reported that the utilization of bare $BaTiO_3$ as the packing material achieved higher NH_3 synthesis rate and energy efficiency without varying any process parameter in plasma-assisted NH_3 synthesis. The reason could be attributed to that the electric field in plasma region was improved in presence of $BaTiO_3$ due to its high dielectric constant [21]. In continuation of our previous work, the transition metal doped M/$BaTiO_3$ catalyst is expected to achieve an improved performance in plasma-assisted NH_3 synthesis since the presence active metal optimized physical-chemical properties of the catalyst.

In this work, the effects of process parameters on plasma-assisted NH_3 synthesis process in a M/$BaTiO_3$ (M = Fe, Co and Ni) packed DBD reactor are reported. Various catalyst characterizations including N_2 adsorption-desorption, X-ray diffraction (XRD) and temperature programmed desorption of CO_2 (CO_2-TPD) are performed to understand the physical-chemical proprieties of M/$BaTiO_3$ catalysts and their effects on plasma-assisted NH_3 synthesis. The central composite design (CCD) model and response surface methodology (RSM) have been proposed to reveal the mutual effects among plasma discharge power, grounded electrode length, catalyst packing ratio and gas flow rate in terms of the NH_3 concentration and energy efficiency of the plasma-assisted NH_3 synthesis process. The analysis of variance (ANOVA) is utilized to quantifiably evaluate the contribution of each process parameter and the potential correlations between them.

2 Experimental

2.1 Experimental setup

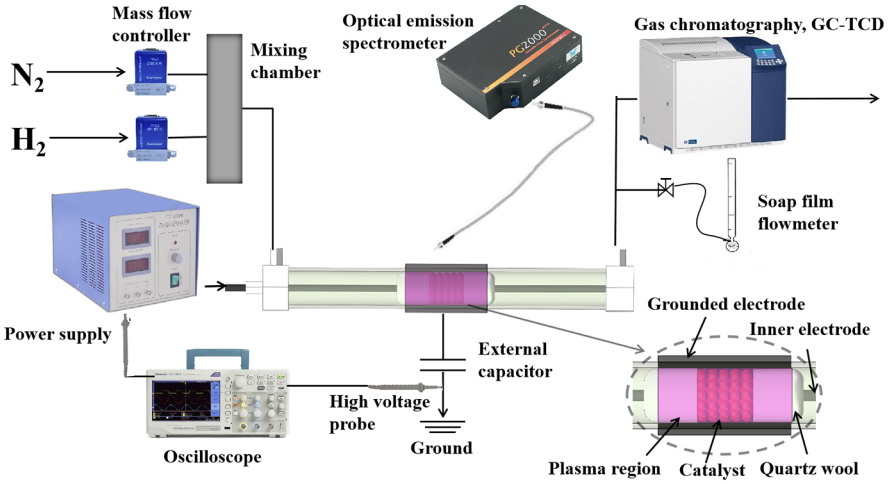

Fig. 1. Experimental setup for the plasma-assisted NH_3 synthesis.

Fig. 1 is the schematic diagram of the experimental set-up. A quartz tube with the inner diameter of 8 mm and the thickness of 2 mm was used as the dielectric barrier. Two PTFE seals were placed at both ends of the quartz tube. A stainless rod with the diameter of 4 mm was used as the high voltage electrode and connected with the power supply (Suman CTP2000K, China). A stainless-steel mesh was wrapped around the quartz tube and used as the grounded electrode. Catalyst samples were placed in the plasma region and fixed by quartz wool. During the experiments, the catalyst preparation and characterization methods were presented in supporting information (Section 1). An external capacitor (C_{ext} = 0.47 μF) was used to determine the quantity of transferred charges (Q_{trans}) during the plasma discharge process. Both the voltage across the external capacitor and the applied voltage across the reactor were measured by high voltage probes (Tektronix TPP0502, USA). All electrical signals were sampled by a four-channel digital oscilloscope (Tektronix TDS2024C, USA). Zero grade (purity > 99.999%) N_2 and H_2 were provided from gas cylinders and regulated by mass flow controllers (Sevenstars D07-B, China). Before being introduced to the reactor, the gas streams were mixed in a mixing chamber. In this work, the molar ratio of N_2 and H_2 was fixed at 1:1. The gas products were analyzed by two-channel gas

chromatography (Fuli 9790II, China) equipped with a thermal conductivity detector (TCD). The optical emission spectra (OES) were measured using an optical spectrometer (Ideaoptics PG2000EX, China).

2.2 Parameter definition and calculation

The discharge power ($P_{\text{dis.}}$) could be calculated as:

$$P_{\text{dis.}}(\text{W}) = f \times C_{\text{ext}} \times A \tag{1}$$

where C_{ext} is external capacitance (0.47 μF) and f is the frequency of AC discharge, and A is the area of the Lissajous figure. In this work, the frequency of AC discharge (f) was kept at 9.5 kHz.

The specific input energy (SIE) of the plasma-assisted process is as follow:

$$SIE(\text{kJ l}^{-1}) = \frac{60 \times P_{\text{dis.}}}{Q} \tag{2}$$

where Q denotes total flow rate (ml min^{-1}).

The energy efficiency of plasma-assisted NH_3 synthesis process is calculated according to the following equation:

$$Energy\ efficiency\left(\text{g kWh}^{-1}\right) = \frac{M \times C_{out} \times Q_{after} \times 60}{P_{\text{dis.}} \times 24} \tag{3}$$

where M denotes the molar mass of NH_3 (g mol^{-1}), C_{out} is the NH_3 concentration measured at the reactor outlet and Q_{after} is the gas flow rate after the reaction, which was measured by a soap-film flowmeter. The coefficient "24" denotes the gas molar volume of 24 l mol^{-1} at the room temperature (around 20 °C), while the coefficient "60" is used to converse minute to second.

The catalyst packing ratio (β) is defined as the ratio of catalyst volume ($V_{\text{cat.}}$) to the volume of plasma discharge region ($V_{\text{dis.}}$), and is calculated by the following equation:

$$\beta\ (\text{vol.\%}) = \frac{V_{\text{cat.}}}{V_{\text{dis.}}} \tag{4}$$

Several electrical parameters were deduced from the Lissajous figure as presented in Fig. S1. In the discharge-off phase (lines DA and CB), the slope presents the total equivalent capacitance of the DBD (C_{cell}). The slope of lines AB and CD presents the effective capacitance (C_{eff}) of the DBD reactor when the filamentary microdischarge presents.

2.3 Experimental design of CCD-RSM

To evaluate the contribution of each independent parameter and their mutual effects on plasma-assisted NH_3 synthesis process, a 4-factor and 5-level CCD model has been employed. In the proposed CCD model, 30 experimental sets were employed for response surface modeling, and the center point was repeated 6 times. The ranges and levels of the four process parameters were given in Table 1. The experimental matrix of the CCD and corresponding experiment results were given in Table S1. ANOVA was carried out to check the adequacy of proposed model. Both CCD experimental design and AVONA analysis were achieved using Matlab.

Table 1. Experimental range and levels of independent variables based on CCD.

Symbols	Variables	Ranges and levels				
		-2	-1	0	1	2
A ($P_{\text{dis.}}$)	Plasma discharge power (W)	5	10	15	20	25
B (F)	Gas flow rate (ml min^{-1})	60	80	100	120	140
C (β)	Catalyst packing ratio (vol.%)	20	40	60	80	100
D (L)	Grounded electrode length (mm)	10	20	30	40	50

3 Results

3.1 Effect of independent process parameters on NH_3 synthesis

3.1.1 Effect of plasma discharge power

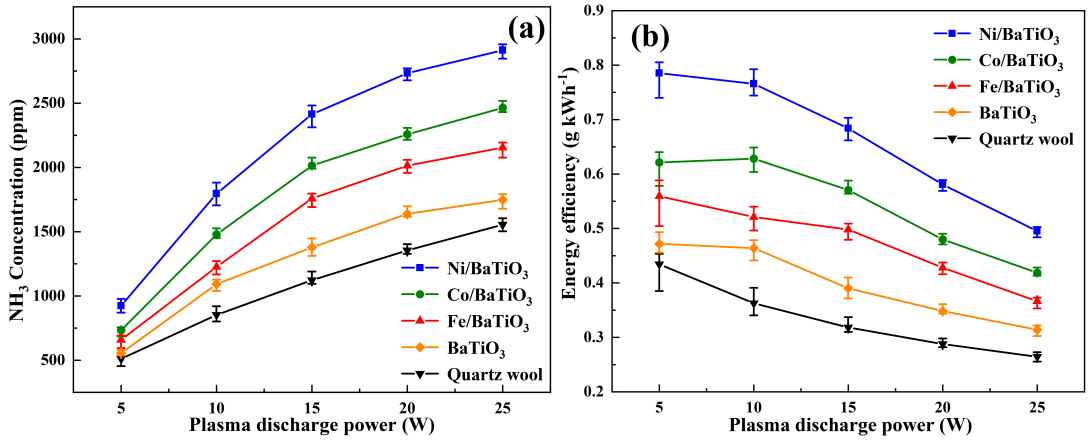

Fig. 2. Effect of plasma discharge power on (a) NH_3 concentration; (b) energy efficiency. (weight of catalyst used = 650 mg, grounded electrode length = 40 mm and gas flow rate = 100 ml min^{-1})

Fig. 2(a) and 2(b) present the effect of plasma discharge power on NH_3 concentration and energy efficiency over different M/$BaTiO_3$ catalysts, respectively. The NH_3 concentration increases significantly as SIE increases irrespective of the catalysts used. On the contrary, a higher plasma discharge power results in decreased energy efficiency.

Quartz wool was used to fix catalysts when employing M/$BaTiO_3$ in this work. The case of quartz wool only acted as a reference group. As with the case of quartz wool only, when plasma discharge power increases from 5 to 25 W, the NH_3 concentration increases from 511 to 1555 ppm while the energy efficiency decreases from 0.43 to 0.26 g kWh^{-1}. Compared with the case of quartz wool packed only, the utilization of $BaTiO_3$ achieves a higher NH_3 concentration, which increases from 555 to 1848 ppm in the same plasma discharge power range. It was widely reported that the presence of active metal could significantly improve the performance in plasma-assisted catalytic processes [14, 22, 23]. In this work, a significant enhancement in NH_3 synthesis performance is also achieved since Fe, Co and Ni were doped on $BaTiO_3$. At a fixed plasma discharge power, the achieved NH_3 concentration and energy efficiency of the process increases in the order of $BaTiO_3$ < Fe/$BaTiO_3$ < Co/$BaTiO_3$ < Ni/$BaTiO_3$. For the case of Ni/$BaTiO_3$, the highest concentration of

2912 ppm and lowest energy efficiency of 0.49 g kWh^{-1} are achieved at the power of 25 W.

3.1.2 Effect of grounded electrode length

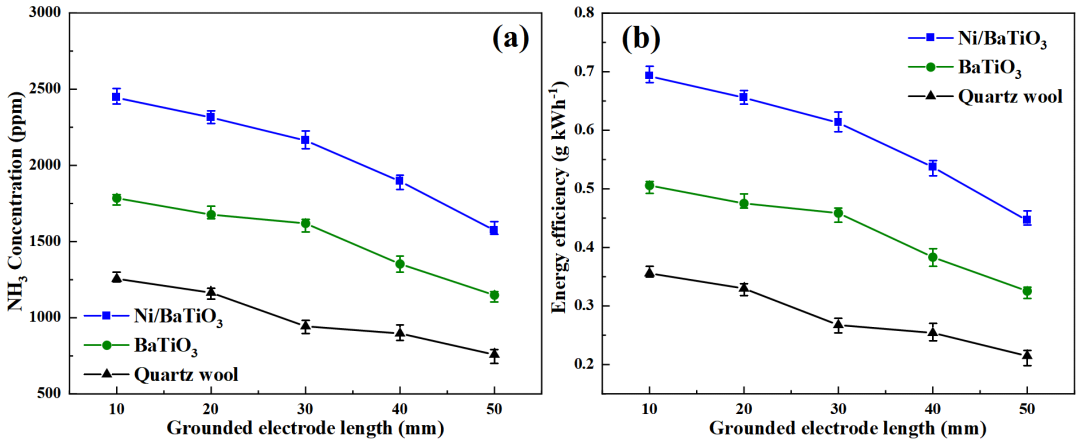

Fig. 3. Effect of grounded electrode length on (a) NH_3 concentration; (b) energy efficiency. (weight of catalyst used = 650 mg, plasma discharge power = 15 W and gas flow rate = 100 ml min^{-1})

The effect of grounded electrode length on NH_3 concentration and energy efficiency is shown in Fig. 3. Surprisingly, as the grounded electrode length increases, the NH_3 concentration presents a trend of monotonically decreasing at a fixed plasma discharge power of 15 W, rather than increases as reported in various plasma-assisted process [24, 25]. For the case of Ni/$BaTiO_3$, when the grounded electrode length is increased from 0 to 50 mm, the NH_3 concentration decreases from 2444 to 1574 ppm. Meanwhile, the energy efficiency decreases from 0.69 to 0.44 g kWh^{-1}. Wang et al. also reported that when the grounded electrode length increased from 100 to 200 mm, the conversion of methane decreased from 20.28% to 13.03% in a micro-DBD plasma reactor at the discharge power of 20 W [26].

Although the increased grounded electrode length would vary the electrical characteristics of plasma (e.g. higher C_{eff} and Q_{trans} with longer grounded electrode as presented in Fig. S2), which may improve the uniformity of plasma and impose positive effects on NH_3 synthesis process.[27, 28] It is also observed that the breakdown voltage dramatically reduces in the DBD reactor with

longer electrode. In particular, when the grounded electrode length increases from 10 to 50 mm, the breakdown voltage decreases from 0.89 to 0.64 kV, indicating a reduction rate of 28% in electric field strength with longer grounded electrode. Meanwhile, the mean electron energy decreases from 1.88 to 1.27 eV and the proportion of energetic electrons in plasma also dramatically decreases (as presented in Fig. S3). The results suggest that the generation of reactive N species is inhibited as the electrode length increases due to the insufficient electron energy for N_2 activation.

3.1.3 Effect of gas flow rate and catalyst packing ratio

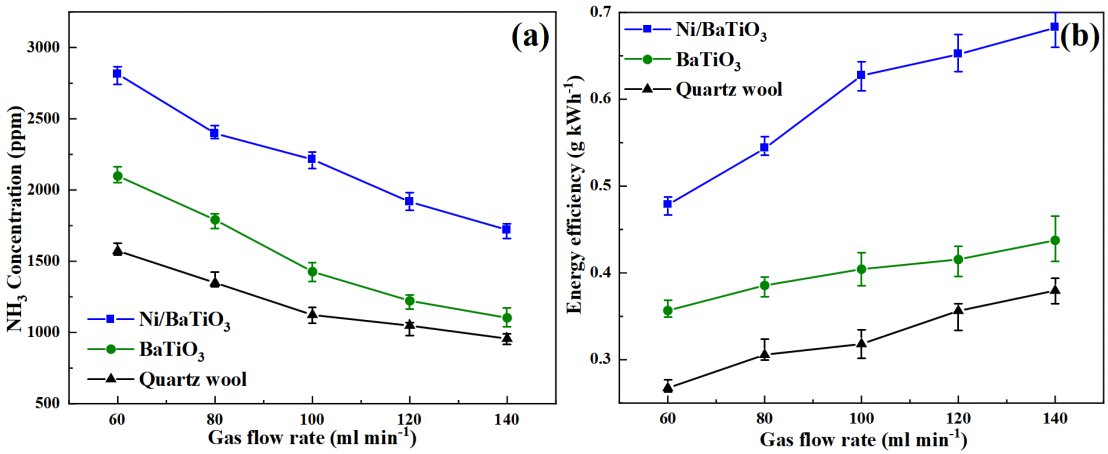

Fig. 4. Effect of gas flow rate on (a) NH_3 concentration; (b) energy efficiency. (weight of catalyst used = 650 mg, grounded electrode length = 40 mm and plasma discharge power = 15 W)

The gas flow rate and catalyst packing ratio are also considered as significant factors affecting NH_3 synthesis performance, as they are directly related to the processing capacity of the DBD reactor [29]. Fig. 4(a) shows the effect of gas flow rate on NH_3 concentration. For the case of $Ni/BaTiO_3$ packed reactor, the NH_3 concentration decreases from 2814 to 1990 ppm when gas flow rate increases from 60 to 140 ml min^{-1}. This phenomenon suggests that at a fixed plasma discharge power, lower gas flow rate is conducive to promote NH_3 generation. The reason could be attributed to the fact that the residence time for each N_2 and H_2 molecule in plasma region is prolonged once the gas flow rate decreases, which leads to higher probabilities for both gas molecule dissociation

and combination of reactive species to generate NH_x (x = 1 or 2) intermediates [30]. The generation of NH_x is the key step of NH_3 formation process in plasma environment [16, 31]. As shown in Fig. 4(b), in contrast to the decreasing trend of NH_3 concentration, the energy efficiency increases as the gas flow rate increases. In the Ni/$BaTiO_3$ packed DBD reactor, as the gas flow rate increases from 60 to 140 ml min^{-1}, the energy efficiency increases from 0.48 to 0.68 g kWh^{-1}. Similar phenomenon was reported by Peng et al. in plasma-assisted NH_3 synthesis process that higher gas flow rate could improve the energy efficiency of NH_3 synthesis [5].

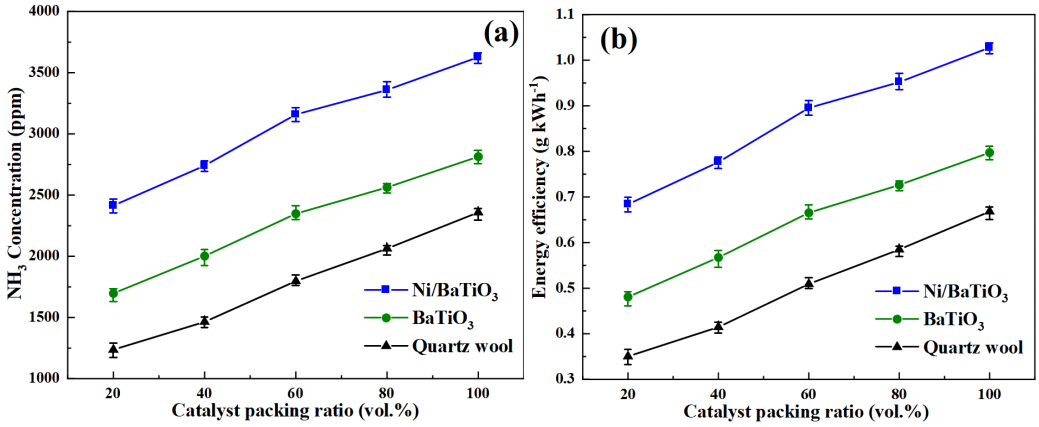

Fig. 5. Effect of catalyst packing ratio on (a) NH_3 concentration; (b) energy efficiency. (plasma discharge power = 15 W, grounded electrode length = 40 mm and gas flow rate = 100 ml min^{-1})

Fig. 5(a) and (b) present the effect of catalyst packing ratio on NH_3 concentration and energy efficiency. The plasma-assisted NH_3 synthesis process was tightly related to the catalyst used amount. Both higher NH_3 concentration and energy efficiency were achieved by increasing catalyst packing ratio at the constant grounded electrode length and gas flow rate. Specifically, with the packing ratio increases from 20 to 100 vol.%, the NH_3 concentration increases from 2414 to 3627 ppm while the energy efficiency increases from 0.68 to 1.03 g kWh^{-1} in presence of Ni/$BaTiO_3$. Similar phenomenon was widely reported in plasma-assisted CO_2 conversion and CO elimination [32, 33].

3.2 Model fitting and ANOVA analysis of CCD-RSM

In this work, the optimization of the plasma-assisted NH_3 synthesis is carried out in the presence of the most active catalyst of $Ni/BaTiO_3$ using the CCD method. The designed experimental matrix and corresponding results are summarized in Table S1. Based on the fitting of experimental data from the designed experimental matrix, polynomial regression models are proposed, which can be summarized as the following equations:

$$Y1 = 113.5 + 401.9A - 22.47083B + 63.12917C - 127.9667D - 0.19187AB - 1.80937AC - 2.25125AD - 0.30297BC - 0.15656BD + 0.58344CD - 1.56958A^2 + 0.18128B^2 - 0.17341C^2 + 2.79885D^2 \quad (5)$$

$$Y2 = - 0.014777 + 0.039632A + 6.15229\times10^{-3}B + 0.017343C - 0.038684D - 1.800094\times10^{-5}AB - 5.69128\times10^{-4}AC - 1.25938\times10^{-3}AD - 8.38445\times10^{-5}BC + 5.40547\times10^{-5}BD + 2.01052\times10^{-4}CD + 5.63349\times10^{-4}A^2 + 1.7394\times10^{-5}B^2 - 4.47792\times10^{-5}C^2 + 8.10425\times10^{-4}D^2 \quad (6)$$

The NH_3 concentration and energy efficiency of the plasma-assisted NH_3 synthesis process are denoted as the responses of "Y1 and Y2", respectively, while the terms of A, B, C and D stand for the factors of plasma discharge power, gas flow rate, catalyst packing ratio and grounded electrode length, respectively. The sign "+" in front of each term in equation (5) and (6) indicates that this term has a positive effect on the corresponding response, while "-" represents its negative effect on the response. The adequacy and significance of the fitting regression models are estimated via the analysis of variance (ANOVA) method as displayed in the following table.

Table 2. ANOVA results for the proposed model

Source	NH_3 Concentration (Y1)			Energy efficiency (Y2)		
	Sum of Squares	F-Value	p-Value	Sum of Squares	F-Value	p-Value
Model	2.22×10^7	145.69	< 0.0001	1.07	49.42	< 0.0001
A	1.53×10^7	1405.77	< 0.0001	0.18	114.79	< 0.0001
B	1.38×10^6	126.61	< 0.0001	0.34	219.99	< 0.0001
C	5.4626×10^4	5.03	0.0405	0.011	7.23	0.0168
D	1.57×10^6	144.20	< 0.0001	0.17	112.67	< 0.0001
AB	5.89×10^3	0.54	0.4728	5.19×10^{-5}	0.034	0.8571

AC	5.24×10^{5}	48.23	< 0.0001	0.052	33.52	< 0.0001
AD	2.03×10^{5}	18.66	0.0006	0.063	41.04	< 0.0001
BC	2.35×10^{5}	21.63	0.0003	0.018	11.64	0.0039
BD	1.5687×10^{4}	1.44	0.2481	1.87×10^{-3}	1.21	0.2887
CD	2.18×10^{5}	20.06	0.0004	0.026	16.73	0.0010
A^2	4.2233×10^{4}	3.89	0.0674	5.44×10^{-3}	3.52	0.0803
B^2	1.44×10^{5}	13.28	0.0024	1.33×10^{-3}	0.86	0.3687
C^2	1.32×10^{5}	12.15	0.0033	8.80×10^{-3}	5.69	0.0307
D^2	2.15×10^{6}	197.82	< 0.0001	0.18	116.53	< 0.0001
Residual	1.63×10^{5}			0.023		
Lack of Fit	1.03×10^{5}	0.85	0.6159	0.018	1.89	0.2500
Pure Error	6.0429×10^{4}			4.85×10^{-3}	5	9.70×10^{-4}
Cor. Total	2.23×10^{7}			1.09	29	
$R^2 = 0.9927$		C.V. % = 3.23		$R^2 = 0.9788$		C.V. % = 4.25
Adj-$R^2 = 0.9859$		Pred-$R^2 = 0.9696$		Adj-$R^2 = 0.9590$		Pred-$R^2 = 0.8970$
Adeq-Precision = 45.902				Adeq-Precision = 26.810		

The p-value is used to evaluate the significance of the model terms. For the best mathematical fitted model, the p-value obtained from ANOVA should be less than 0.05 [34]. The F-value is the ratio of "mean square" to "residual" of the model. The p-value of both NH_3 concentration (F-value = 145.69) and energy efficiency (F-value = 49.42) are less than 0.0001, indicating that the models are statistically significant in fitting the experimental data with the Fischer's F-test [35]. The veracity for proposed models can also been confirmed by the p-value of the "Lack of Fit". The p-values of "Lack of Fit" are 0.6159 and 0.2500 for the terms of NH_3 concentration and energy efficiency, respectively, implying that the value of "lack of fit" is not significant and the proposed model is proved to have the high capability of prediction.

The correlation coefficients of R^2 and Adj-R^2 could be used to determine the matching quality between the experimental data and proposed model [36]. The R^2 and Adj-R^2 of the proposed models for NH_3 concentration are 0.9927 and 0.9859, respectively, while the values are 0.9788 and 0.9590 for the energy efficiency, respectively. A high R^2 value above 0.90 is preferred for a mathematical

fitted model [37]. The differences between Adj-R^2 and Pred-R^2 of the fitting models for both NH_3 concentration and energy efficiency is less than 0.2, advocating the stability and validity for the regression models [38].

The relative dispersion for these experimental points from the prediction based on the model can be determined by the coefficient of variation (C.V.), which should not be higher than 10% [12]. In the proposed model, low C.V. values for NH_3 concentration (3.23%) and energy efficiency (4.25%) confirm the experimental results are of high repeatability. The values of "Adeq-Precision" reach 46.902 for NH_3 concentration and 26.810 for energy efficiency, indicating that the proposed models could fit experimental data well and the signal to noise ratio is adequate (>4) [39]. Hence, the proposed polynomial regression models are demonstrated to be satisfactorily fitted to the experimental data.

4 Discussions

4.1 Mechanisms of plasma-assisted NH_3 synthesis over Ni/$BaTiO_3$

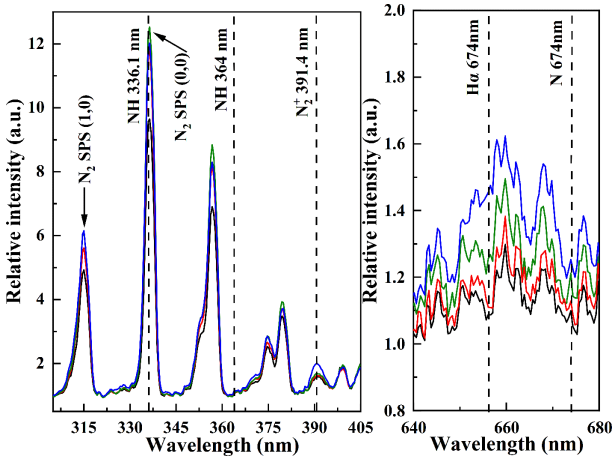

Fig. 6. Optical emission spectra for N_2-H_2 plasma over M/$BaTiO_3$.
(weight of catalyst used = 650 mg, grounded electrode length = 40 mm, gas flow rate = 100 ml min^{-1} and plasma discharge power = 15 W)

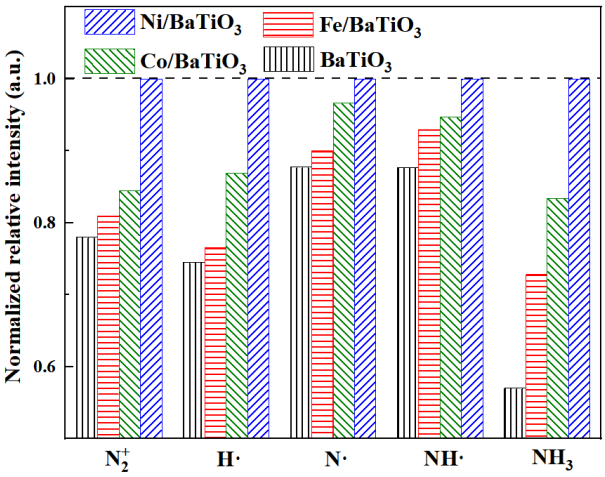

Fig. 7. Normalized relative intensity of N_2^+, H·, N·, NH· and NH_3 in plasma-assisted NH_3 synthesis.
(weight of catalyst used = 650 mg, grounded electrode length = 40 mm, gas flow rate = 100 ml min^{-1} and plasma discharge power = 15 W)

Optical emission spectra (Fig. 6) were measured to determine the relative concentration of reactive species in the presence of $M/BaTiO_3$. The selected characterization peaks in determining of reactive species (i.e. N·, H·, N_2^+ and NH·) were illustrated in section 5 of supporting information. In order to compare the relative concentration of the reactive species, the intensities of N·, H·, N_2^+ and NH· spectrum lines in the presence of $M/BaTiO_3$ were normalized and presented in Fig. 7. The relative maximum concentration for these reactive species is obtained in the presence of $Ni/BaTiO_3$. Among the $M/BaTiO_3$ catalysts, the normalized relative concentration of N·, H·, NH· and N_2^+ following the order of $BaTiO_3$ < $Fe/BaTiO_3$ < $Co/BaTiO_3$ < $Ni/BaTiO_3$. During the heterogeneous catalytic reaction of plasma-assisted NH_3 synthesis, reactions that taking place on the catalyst surfaces are believed to significantly enhance the reaction rate via interactions between the reactants and active sites on the surface of the catalyst [40]. These active sites operate via E-R (Eley-Rideal) and L-H (Langmuir-Hinshelwood) mechanisms, i.e. reactive species (e.g. NH_x, H_α, N_2^+, etc.) could be adsorbed from gas phase onto the surface of catalyst to improve the localized concentration of reactants for NH_3 synthesis [16]. The results in Fig. 7 indicate that compared with other catalyst

samples, more reactive species were generated in the presence of Ni/$BaTiO_3$. These reactive species could be involved in surface reactions, react with each other and tend to generate NH_x species to promote NH_3 synthesis [41].

The doped metal significantly improved total pore volume and average pore size of the obtained catalysts (as listed in Table S3). The reason could be attributed to the porous metal oxide on the surface of catalyst, which brings more micro-pores to catalysts and benefits NH_3 synthesis [18, 42]. As presented in Fig. S5, the unvaried XRD patterns suggest that during the preparation process of M/$BaTiO_3$, the structure of $BaTiO_3$ support was maintained, while its high dielectric constant could enhance the electric field during plasma discharge process. Our previous work also reported that the performance of plasma-assisted NH_3 synthesis is closely correlated to the basicity of the catalysts [43, 44]. The results from CO_2-TPD profiles (as presented in Fig. S6) suggest that the Ni/$BaTiO_3$ has the highest amount of basicity and abundant strong basic sites. The basic sites acted as the role of an electron donor that tend to transfer electrons to active metal near the basic sites and therefore promote the metal to be an electron-enriched state. When N_2 was chemically adsorbed on active metal surface, the electron could be transferred to the π^*-antibonding orbital of N_2 molecule, and therefore weaken nitrogen triple bond [45, 46]. Afterwards, the dissociation of N_2 could be facilitated and further promote NH_3 synthesis.

Furthermore, the bonding energy of metal-nitrogen (M-N) bonds for Fe, Co and Ni follows the order of Fe > Co > Ni [47]. The dissociative adsorption of NH_3 on the catalyst surface would occur more easily with a stronger M-N bond, since a lower M-N bond energy would contribute to NH_3 synthesis by promoting the desorption of formed NH_3 form catalyst surface [16]. The order of NH_3 concentration in plasma-assisted reactions over M/$BaTiO_3$ follows the order of Ni/$BaTiO_3$ >

$Co/BaTiO_3$ > $Fe/BaTiO_3$, which is in accordance with the descent trend of M-N bond energy. This phenomenon suggests the use of Ni may improve NH_3 synthesis rate by inhibiting the decomposition of NH_3.

4.2 The mutual effects of the process parameters on responses

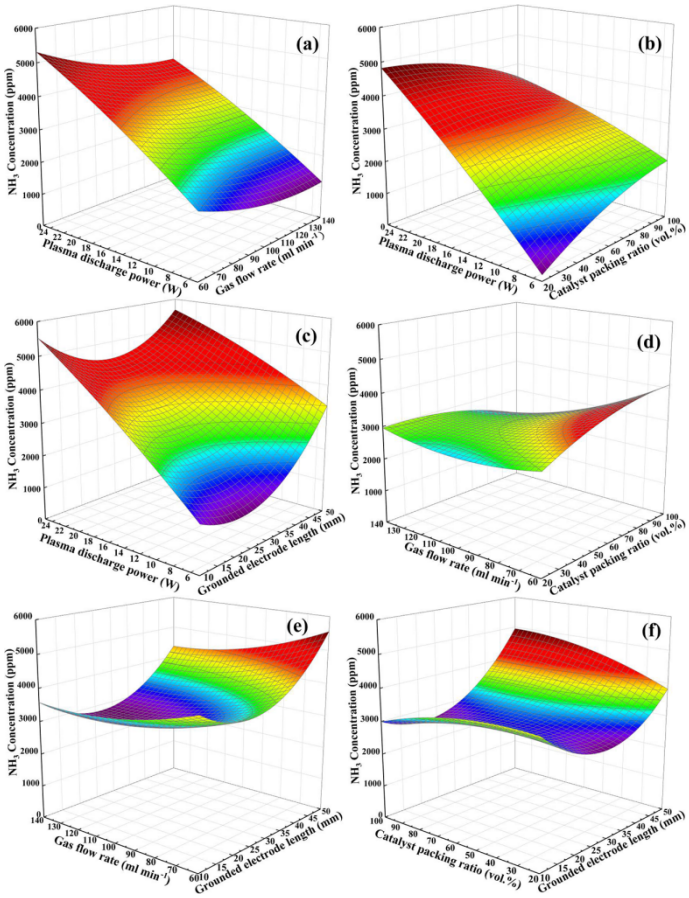

Fig. 8. The response surface plots of the interaction between process parameters on the response of NH_3 concentration.

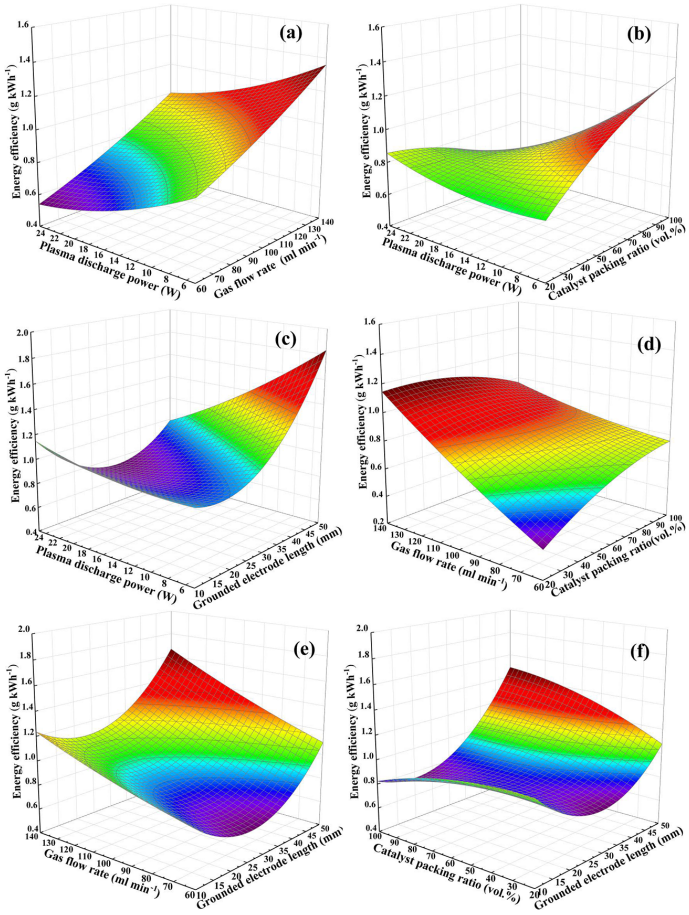

Fig. 9. The response surface plots of the interaction between process parameters on the response of energy efficiency.

Fig. 8 and 9 are the response surface plots of NH_3 concentration and energy efficiency over Ni/$BaTiO_3$ catalyst, respectively. Considering the contribution of each independent variable, it is visible that the NH_3 concentration and energy efficiency are more remarkably affected by plasma discharge power and gas flow rate, respectively. The dominant contribution of plasma discharge power on NH_3 concentration can also be confirmed by the highest F-value of 1405.77 among the four independent variables. The effect of gas flow rate and grounded electrode length is also significant to both NH_3 concentration and energy efficiency due to their high F-value.

As presented in Fig. 8(a) and 9(a), as plasma discharge power increases, NH_3 concentration decreases whereas the energy efficiency increases continuously. The increase trend of NH_3 concentration with plasma discharge power can be ascribed that the generation of more intense

discharge filaments and energetic electrons occurs with increasing discharge power, which in turn promotes the generation of chemically reactive species, e.g. N· and H· [23, 48, 49]. The decrease in energy efficiency can be explained by the following aspects: (1) Under the condition of high plasma discharge power, the increased power dissipated into the synthesis reaction might not be enough to increase the synthesis rate of NH_3, which caused the plateau in NH_3 concentration and a relatively dramatic decrease in energy efficiency [50]. (2) The electron-impact NH_3 decomposition was aggravated at high plasma discharge power and led to a waste of energy [21]. (3) High plasma discharge power led to a temperature increase within the plasma region, which may cause a low energy utilization and inhibit forward reaction of NH_3 synthesis [6, 21, 51].

As presented in Fig. 8(b) and 9(b), both high plasma discharge power and catalyst packing ratio present positive effect in NH_3 concentration and energy efficiency. However, under the condition of high plasma discharge power, the energy efficiency turns to decrease with the increasing catalyst packing ratio. It is well known that in a plasma-catalysis system, chemically reactive species have two reaction pathways of (1) homogeneous reaction in gas phase; (2) heterogeneous reaction with adsorbed species onto the catalyst surface via E-R and L-H mechanisms. In both cases, the reactive species undergo complex reactions with each other to form the NH_3 [14]. For the gas phase reactions, with the increasing plasma discharge power, mean electron energy and probability of the generation of high energetic electrons would increase. The improved electron energy could promote the dissociation of N_2 and H_2, contributing the generation of reactive species, e.g. N·, H· and NH_x radicals in gas phase. The heterogeneous pathways are greatly dependent on catalysts. As the catalyst packing ratio increases, more active sites could be introduced to plasma region and available for the surface-involved reactions in plasma region. With the increasing amount of catalyst packed

in plasma region, the possibilities for the dissociative adsorption of N_2 and H_2 on catalyst surface could be effectively improved. These dissociative adsorption reactions on catalyst surface could improve the localized concentration of reactive species, and therefore promote the formation of NH_x species in kinetics through heterogeneous reactions [52].

Such an enhancement of energy efficiency with catalyst packing ratio could not always be observed. On one hand, an increasing packing ratio of M/$BaTiO_3$ could enhance the electric field without varying any other parameters, and hence be advantageous to the NH_3 synthesis under the suitable plasma discharge power. On the other hand, once the plasma discharge power was higher than the optimum value, the increasing amount of M/$BaTiO_3$ would result in an excessive electric field due to its high dielectric constant, which further aggravates electron-impact NH_3 decomposition and is responsible for the descending NH_3 concentration and energy efficiency, which has been detailed discussed in our previous work [21]. Hence, as presented in Fig. 8(b), increasing catalyst packing ratio could significantly promote NH_3 synthesis then achieve a higher NH_3 concentration even at a lower plasma discharge power. But at higher plasma discharge power, the increased catalyst packing ratio may result in a descending trend of NH_3 concentration due to the aggravation of NH_3 decomposition and inhibition of NH_3 formation.

The results in Fig. 8(c) and Fig. 9(c), both NH_3 concentration and energy efficiency presence the U-shaped curves as electrode length increases. Since the catalyst packing ratio is fixed, the increasing grounded electrode length not only leads to an enlarged plasma region, but also more catalyst used in plasma region. To some extent, this situation is similar to that increasing the catalyst packing ratio only, but the insufficient electron energy would be exaggerated due to the enlarged plasma region at a fixed plasma discharge power, and thus lead to a dramatically decrement in NH_3

concentration and energy efficiency initially. With the further increasing grounded electrode length, both NH_3 concentration and energy efficiency turns from decrease to increase, which may be attributed to that the increasing the amount of catalyst exposes more active sites in plasma region and promotes NH_3 formation through heterogeneous reaction. Since the p-value for NH_3 concentration and energy efficiency are both lower than 0.05, the F-values of term "AD" for NH_3 concentration (18.66) and energy efficiency (41.04) indicate that the effect of "AD" is more significant on energy efficiency.

The results in Fig. 8(d) and 9(d) indicate that as gas flow rate increases, the NH_3 concentration decreases whereas the energy efficiency increases. With the increasing number of N_2 and H_2 molecules flowed into plasma region at higher gas flow rate, more gas molecules could be activated when flow through plasma region per unit time. Afterwards, the possibilities of effective collisions between N and H reactive species increase, leading to higher NH_3 production rate. Therefore, a higher energy efficiency could be achieved by increasing gas flow rate. It is also reported by Xie et al. that in the packed-bed DBD reactor, the external diffusion resistance of N_2 and H_2 gases on the catalyst was reduced with increasing gas flow rate, which improved the reaction rate of NH_3 synthesis [53].

4.3 Comparison of optimized reaction performance with other literature

The optimum working condition for plasma-assisted NH_3 synthesis are determined by the proposed model based on the energy efficiency. The predicted optimum condition for energy efficiency is $P_{dis.}$ = 5 W, F = 139.33 ml min^{-1}, β = 100 vol.% and L = 50 mm, while the predicted

maximum energy efficiency is 2.37 g kWh^{-1}. The experiments were conducted under the above predicted optimum conditions for three times in order to confirm the validity of the proposed model. The obtained energy efficiency is 2.35 g kWh^{-1} with a relative error of 3.4% to 3.0%, implying the well matching between the actual results and the predicted results from the proposed model.

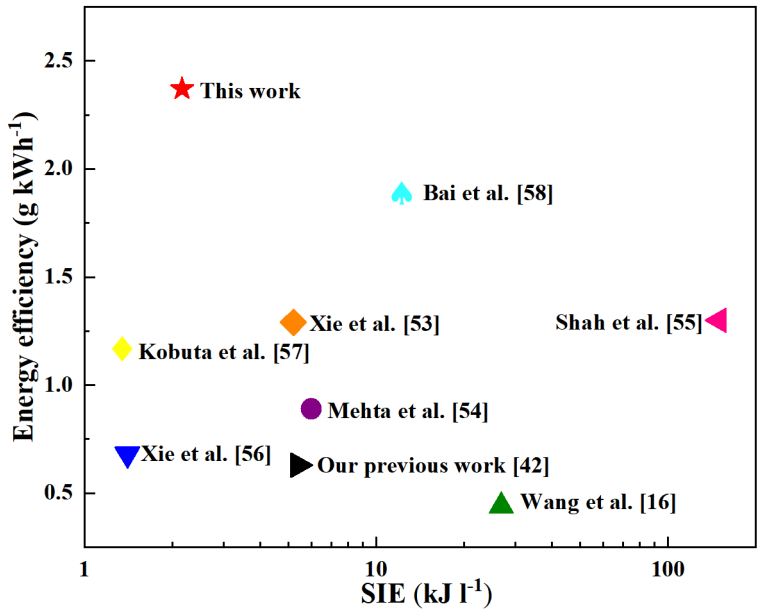

Fig. 10. Comparison of economic performances of plasma-assisted NH_3 synthesis with previous studies.

A comparison of economic performance of the plasma-assisted NH_3 synthesis process is presented in Fig. 10. The economic performance was assessed in term of the highest energy efficiency reported in previous works. Mehta et al. reported that the energy efficiency for DBD plasma assisted NH_3 synthesis using Ni/Al_2O_3 was 0.89 g kWh^{-1}, almost twice of that using Al_2O_3 support at the same SIE of 6.0 kJ l^{-1} [54]. Shah et al. reported that the peak energy efficiency for energy synthesis using Ni-MOF-74 as catalyst was 1.3 g kWh^{-1} at 50 W in the RF plasma-catalysis system [55]. Wang et al. achieved the energy efficiency of 0.44 g kWh^{-1} in a DBD reactor using Ni/Al_2O_3 at the SIE of 26.8 kJ l^{-1} [16]. Xie et al. reported the maximum yield of 0.68 g kWh^{-1} in their work occurs at the energy density of 1.4 kJ l^{-1} in the Ru/Al_2O_3-packed DBD reactor [56]. It was also Xie et al. that using Ru/L-MgO packed DBD reactor obtained a higher energy yield of 1.29

g kWh^{-1} at 5.2 kJ l^{-1} compared to that (~0.3 g kWh^{-1}) in the case of plasma only [53]. Our previous work reported that the highest energy yield of 0.63 g kWh^{-1} is achieved at an SIE of 5.4 kJ l^{-1} using Ru/AC in a DBD reactor, which is 21.2% higher than that of using the Ru/ZSM-5 catalyst [42]. Koubuta et al. achieved the energy efficiency of 1.16 g kWh^{-1} using microwave plasma at high temperature of 790–1240 K [57]. Bai et al. achieved their greatest energy efficiency using a microgap DBD reactor, which the surface of barrier is sprayed α-A_2O_3 layer [58]. In this work, the highest energy efficiency at the predicted optimum condition obtained from proposed model is 2.37 g kWh^{-1} at 2.16 kJ l^{-1} using Ni/$BaTiO_3$ in a DBD reactor. Compared with the presented works, a competitive energy efficiency was achieved after process optimization using CCD-RSM in this work. The promising opportunities for further improvement in economic performance are expected to hinge on the development of effective catalysts specialized in plasma-assisted NH_3 synthesis process using RSM.

5 Conclusions

Plasma-assisted NH_3 synthesis has been conducted over transition metal (M = Fe, Co and Ni) doped M/$BaTiO_3$ catalyst at ambient temperature and pressure. The presence of M/$BaTiO_3$ catalyst significantly enhanced NH_3 concentration and energy efficiency, compared that using plasma alone. In this work, the NH_3 concentration was observed in the order of Ni/$BaTiO_3$ > Co/$BaTiO_3$ > Fe/$BaTiO_3$ > $BaTiO_3$. The highest NH_3 concentration of 2192 ppm and energy efficiency of 0.78 g kWh^{-1} were achieved at 25 W and 5 W in the presence of Ni/$BaTiO_3$, respectively. Compared at the same operation condition of 25W and 100 ml min^{-1}, the NH_3 concentration and energy efficiency achieved by packing Ni/$BaTiO_3$ were around 1.9 times higher than that of quartz wool. The

enhanced performance of Ni/$BaTiO_3$ could be attributed to the abundant basic sites and weaker M-N bond on its surface, which could benefit the dissociation reactions to generate reactive species in plasma environment together with the desorption of formed NH_3. The higher specific surface area and pore volume would also be responsible for the higher NH_3 concentration and energy efficiency in presence of Ni/$BaTiO_3$.

The interactions between process parameters on NH_3 concentration and energy efficiency were systematically studied by CCD-RSM. The results of AVONA analysis indicated that the plasma discharge power and discharge length have more pronounced effect on NH_3 concentration, whereas gas flow rate and plasma discharge power play a dominant role in energy efficiency. Based on the proposed model, the predicted optimum energy efficiency of 2.37 g kWh^{-1} could be achieved at the working conditions of $P_{dis.}$ = 5 W, F = 139.33 ml min^{-1}, β = 100 vol.% and L = 50 mm, which is much higher than the energy efficiency from various literature.

Acknowledgments

The authors are grateful for the financial support from National Natural Science Foundation of China (No.51976093) and K.C. Wong Magna Fund in Ningbo University.

References

[1] C. Mounaïm-Rousselle, P. Brequigny, Ammonia as fuel for low-carbon spark-ignition engines of tomorrow's passenger cars, Front. Mech. Eng. 6 (2020). DOI: 10.3389/fmech.2020.00070

[2] A. Sánchez, M. Martín, P. Vega, Biomass based sustainable ammonia production: Digestion vs gasification, ACS Sustainable Chem. Eng. 7(11) (2019) 9995-10007. DOI: 10.1021/acssuschemeng.9b01158

[3] Y. Yao, J. Wang, U.B. Shahid, M. Gu, H. Wang, H. Li, M. Shao, Electrochemical synthesis of ammonia from nitrogen under mild conditions: Current status and challenges, Electrochem. Energy Rev. 3(2) (2020) 239-270. DOI: 10.1007/s41918-019-00061-3

[4] P. Peng, P. Chen, C. Schiappacasse, N. Zhou, E. Anderson, D. Chen, J. Liu, Y. Cheng, R. Hatzenbeller, M. Addy, Y. Zhang, Y. Liu, R. Ruan, A review on the non-thermal plasma-assisted ammonia synthesis technologies, J. Cleaner Prod. 177 (2018) 597-609. DOI: 10.1016/j.jclepro.2017.12.229

[5] P. Peng, Y. Li, Y.L. Cheng, S.B. Deng, P. Chen, R. Ruan, Atmospheric pressure ammonia synthesis using non-thermal plasma assisted catalysis, Plasma Chem. Plasma Process. 36(5) (2016) 1201-1210. DOI: 10.1007/s11090-016-9713-6

[6] S. Li, T. van Raak, F. Gallucci, Investigating the operation parameters for ammonia synthesis in dielectric barrier discharge reactors, J. Phys. D: Appl. Phys. 53(1) (2020). DOI: 10.1088/1361-6463/ab4b37

[7] M. Bai, X. Bai, Z. Zhang, M. Bai, Synthesis of ammonia in a strong electric field discharge at ambient pressure, Plasma Chem. Plasma Process. 53(1) (2020). DOI: 10.1088/1361-6463/ab4b37

[8] J. Liu, X. Zhu, X. Hu, F. Zhang, X. Tu, Plasma-assisted ammonia synthesis in a packed-bed dielectric barrier discharge reactor: effect of argon addition, Vacuum 197 (2022). DOI: 10.1016/j.vacuum.2021.110786

[9] A.H. Khoja, M. Tahir, N.A. Saidina Amin, Process optimization of DBD plasma dry reforming of methane over Ni/$La_2O_3MgAl_2O_4$ using multiple response surface methodology, Int. J. Hydrogen Energy 44(23) (2019) 11774-11787. DOI: 10.1016/j.ijhydene.2019.03.059

[10] D.H. Mei, S.Y. Liu, X. Tu, CO_2 reforming with methane for syngas production using a dielectric barrier discharge plasma coupled with Ni/γ-Al_2O_3 catalysts: Process optimization through response surface methodology, J. CO_2 Util. 21 (2017) 314-326. DOI: 10.1016/j.jcou.2017.06.020

[11] N. Jiang, Y. Zhao, K. Shang, N. Lu, J. Li, Y. Wu, Degradation of toluene by pulse-modulated multistage DBD plasma: Key parameters optimization through response surface methodology (RSM) and degradation pathway analysis, J. Hazard. Mater. 393 (2020) 122365. DOI: 10.1016/j.jhazmat.2020.122365

[12] T. Chang, Z. Shen, C. Ma, J. Lu, Y. Huang, S.K.P. Veerapandian, N. De Geyter, R. Morent, Process optimization of plasma-catalytic formaldehyde removal using MnOx–Fe_2O_3 catalysts by response surface methodology, J. Environ. Chem. Eng. 9(4) (2021). DOI: 10.1016/j.jece.2021.10577

[13] M.S. Souza, R.S. Araujo, A.C. Oliveira, Optimizing reaction conditions and experimental studies of selective catalytic reduction of NO by CO over supported SBA-15 catalyst, Environ. Sci. Pollut. Res. Int 27(24) (2020) 30649-30660. DOI: 10.1007/s11356-020-09391-y

[14] B.S. Patil, N. Cherkasov, N.V. Srinath, J. Lang, A.O. Ibhadon, Q. Wang, V. Hessel, The role of heterogeneous catalysts in the plasma-catalytic ammonia synthesis, Catal. Today 362 (2021) 2-10. DOI: 10.1016/j.cattod.2020.06.074

[15] B.S. Patil, N. Cherkasov, J. Lang, A.O. Ibhadon, V. Hessel, Q. Wang, Low temperature plasma-catalytic NOx synthesis in a packed DBD reactor: Effect of support materials and supported active metal oxides, Appl. Catal., B 194 (2016) 123-133. DOI: 10.1016/j.apcatb.2016.04.055

[16] Y. Wang, M. Craven, X. Yu, J. Ding, P. Bryant, J. Huang, X. Tu, Plasma-enhanced catalytic synthesis of ammonia over a Ni/Al_2O_3 catalyst at near-room temperature: Insights into the importance of the catalyst surface on the reaction mechanism, ACS Catal. 9(12) (2019) 10780-10793. DOI: 10.1021/acscatal.9b02538

[17] F.A. Herrera, G.H. Brown, P. Barboun, N. Turan, P. Mehta, W.F. Schneider, J.C. Hicks, D.B. Go, The impact of transition metal catalysts on macroscopic dielectric barrier discharge (DBD)

characteristics in an ammonia synthesis plasma catalysis reactor, J. Phys. D: Appl. Phys 52(22) (2019). DOI: 10.1088/1361-6463/ab0c58
[18] C. Srilakshmi, G.M. Rao, R. Saraf, Effect of the nature of a transition metal dopant in $BaTiO_3$ perovskite on the catalytic reduction of nitrobenzene, RSC Adv. 5(57) (2015) 45965-45973. DOI: 10.1039/C5RA06864A
[19] P. Araújo, K. Costa, F.B. Passos, Hydrogen production from methane autothermal reforming over $CaTiO_3$, $BaTiO_3$ and $SrTiO_3$ supported nickel catalysts, Int. J. Hydrogen Energy 46(47) (2021). DOI: 10.1016/j.ijhydene.2021.04.202
[20] W. Liang, L. Ma, H. Liu, J. Li, Toluene degradation by non-thermal plasma combined with a ferroelectric catalyst, Chemosphere 92(10) (2013) 1390-1395. DOI: 10.1016/j.chemosphere.2013.05.042
[21] J. Liu, X. Zhu, X. Hu, X. Tu, Plasma-assisted ammonia synthesis in a packed-bed dielectric barrier discharge reactor: roles of dielectric constant and thermal conductivity of packing materials, Plasma Sci. Technol. 24(2) (2022) 025503. DOI: 10.1088/2058-6272/ac39fb
[22] X. Tu, H.J. Gallon, M.V. Twigg, P.A. Gorry, J.C. Whitehead, Dry reforming of methane over a Ni/Al_2O_3 catalyst in a coaxial dielectric barrier discharge reactor, J. Phys. D: Appl. Phys. 44(27) (2011). DOI: 10.1088/0022-3727/44/27/274007
[23] B.S. Patil, A.S.R. van Kaathoven, F.J.J. Peeters, N. Cherkasov, J.G. Lang, Q. Wang, V. Hessel, Deciphering the synergy between plasma and catalyst support for ammonia synthesis in a packed dielectric barrier discharge reactor, J. Phys. D: Appl. Phys 53(14) (2020). DOI: 10.1088/1361-6463/ab6a36
[24] S. Li, X. Dang, X. Yu, G. Abbas, Q. Zhang, L. Cao, The application of dielectric barrier discharge non-thermal plasma in VOCs abatement: A review, Chem. Eng. J. 388 (2020). DOI: 10.1016/j.cej.2020.124275
[25] S. Nemmich, A. Tilmatine, Z. Dey, N. Hammadi, K. Nassour, S. Messal, Optimal sizing of a DBD ozone generator using response surface modeling, Ozone: Sci. Eng. 37(1) (2015) 3-8. DOI: 10.1080/01919512.2014.939743
[26] B. Wang, W. Yan, W. Ge, X. Duan, Methane conversion into higher hydrocarbons with dielectric barrier discharge micro-plasma reactor, J. Energy Chem. 22(6) (2013) 876-882. DOI: 10.1016/S2095-4956(14)60267-9
[27] D. Mei, X. Zhu, Y. He, J. Yan, X. Tu, Plasma-assisted conversion of CO_2 in a dielectric barrier discharge reactor: understanding the effect of packing materials, Plasma Sources Sci. Technol. 24(1) (2014). DOI: 10.1088/0963-0252/24/1/015011
[28] Y. Zeng, X. Tu, Plasma-catalytic hydrogenation of CO_2 for the cogeneration of CO and CH_4 in a dielectric barrier discharge reactor: effect of argon addition, J. Phys. D: Appl. Phys. 50(18) (2017). DOI: 10.1088/1361-6463/aa64bb
[29] A.H. Khoja, M. Tahir, N. Amin, Dry reforming of methane using different dielectric materials and DBD plasma reactor configurations, Energy Convers. Manage. 144(15) (2017). DOI: 10.1016/j.enconman.2017.04.057
[30] X. Zhu, D. Mei, C. Zheng, J. Zhou, X. Gao, Investigation of hybrid plasma-catalytic removal of acetone over $CuO/\gamma\text{-}Al_2O_3$ catalysts using response surface method, Chemosphere 155 (2016) 9-17. DOI: 10.1016/j.chemosphere.2016.03.114
[31] L.R. Winter, B. Ashford, J. Hong, A.B. Murphy, J.G. Chen, Identifying surface reaction intermediates in plasma catalytic ammonia synthesis, ACS Catal. 10(24) (2020) 14763-14774. DOI:

10.1021/acscatal.0c03166
[32] C. Chang, T. Lin, Elimination of Carbon Monoxide in the Gas Streams by Dielectric Barrier Discharge Systems with Mn Catalyst, Plasma Chem. Plasma Process. 25(4) (2005) 387-401. DOI: 10.1007/s11090-004-3135-6
[33] J. Li, S. Zhu, K. Lu, C. Ma, F. Yu CO_2 conversion in a coaxial dielectric barrier discharge plasma reactor in the presence of mixed ZrO_2-CeO_2, J. Environ. Chem. Eng. 9(6) (2020) 104654. DOI: 10.1016/j.jece.2020.104654
[34] A. Auo, B. Ce, C. Odo, D. En, B. Csu, Modeling and optimization of african pear seed oil esterification and transesterification using artificial neural network and response surface methodology comparative analysis, Ind. Crops Prod. 140(15) 2019 111707-111707. DOI: 10.1016/j.indcrop.2019.111707
[35] N. Jiang, Y. Zhao, C. Qiu, K. Shang, N. Lu, J. Li, Y. Wu, Y. Zhang, Enhanced catalytic performance of CoO-CeO_2 for synergetic degradation of toluene in multistage sliding plasma system through response surface methodology (RSM), Appl. Catal., B 259 (2019) 118061. DOI: 10.1016/j.apcatb.2019.118061
[36] L.A. Fakhri, B. Ghanbarzadeh, J. Dehghannya, F. Abbasi, H. Ranjbar, Optimization of mechanical and color properties of polystyrene/nanoclay/ nano ZnO based nanocomposite packaging sheet using response surface methodology, Food Packag. Shelf Life 17 (2018) 11-24. DOI: 10.1016/j.fpsl.2018.04.005
[37] U. Javed, R. Farooq, F. Shehzad, Z. Khan, Optimization of HNO_3 leaching of copper from old AMD Athlon processors using response surface methodology, J. Environ. Manage. 211(1) (2018) 22-27. DOI: 10.1016/j.jenvman.2018.01.026
[38] A. Me, A. Aeb, A. Kke, A. Amr, B. Hp, C. Kks, D. Ms, E. Mi, Maximization of biodiesel production from sunflower and soybean oils and prediction of diesel engine performance and emission characteristics through response surface methodology, Fuel 266(15) 2020 117072. DOI: 10.1016/j.fuel.2020.117072
[39] J. Li, Q. Liu, Q.q. Ji, B. Lai, Degradation of p-nitrophenol (PNP) in aqueous solution by Fe0-PM-PS system through response surface methodology (RSM), Appl. Catal., B 200 (2017) 633-646. DOI: 10.1016/j.apcatb.2016.07.026
[40] J. Shah, W. Wang, A. Bogaerts, M.L. Carreon, Ammonia synthesis by radio frequency plasma catalysis: Revealing the underlying mechanisms, ACS Appl. Energy Mater. 1(9) (2018) 4824-4839. DOI: 10.1021/acsaem.8b00898
[41] J. Hong, S. Pancheshnyi, E. Tam, J.J. Lowke, S. Prawer, A.B. Murphy, Kinetic modelling of NH_3 production in N_2-H_2 non-equilibrium atmospheric-pressure plasma catalysis, J. Phys. D: Appl. Phys. 50(15) (2017) 154005. DOI: 10.1088/1361-6463/aa6229
[42] X. Zhu, J. Liu, X. Hu, Z. Zhou, X. Li, W. Wang, R. Wu, X. Tu, Plasma-catalytic synthesis of ammonia over Ru-based catalysts: Insights into the support effect, J. Energy Inst. 102 (2022) 240-246. DOI: 10.1016/j.joei.2022.02.014
[43] X. Zhu, X. Hu, X. Wu, Y. Cai, H. Zhang, X. Tu, Ammonia synthesis over γ-Al_2O_3 pellets in a packed-bed dielectric barrier discharge reactor, J. Phys. D: Appl. Phys 53(16) (2020) 164002. DOI: 10.1088/1361-6463/ab6cd1
[44] X. Hu, X. Zhu, X. Wu, Y. Cai, X. Tu, Plasma-enhanced NH_3 synthesis over activated carbon-based catalysts: Effect of active metal phase, Plasma Processes Polym. 17(12) (2020). DOI: 10.1002/ppap.202000072

[45] M. Kitano, Y. Inoue, Y. Yamazaki, F. Hayashi, S. Kanbara, S. Matsuishi, T. Yokoyama, S.W. Kim, M. Hara, H. Hosono, Ammonia synthesis using a stable electride as an electron donor and reversible hydrogen store, Nat. Chem. 4(11) (2012) 934-940. DOI: 10.1038/nchem.1476
[46] A. Tarka, W. Patkowski, M. Zybert, H. Ronduda, W. Raróg-Pilecka, Synergistic Interaction of Cerium and Barium-New Insight into the Promotion Effect in Cobalt Systems for Ammonia Synthesis, Catalysts 10(6) (2020) 658. DOI: 10.3390/catal10060658
[47] J. Shah, F. Gorky, P. Psarras, B. Seong, D.A. Gómez-Gualdrón, M.L. Carreon, Enhancement of the yield of ammonia by hydrogen-sink effect during plasma catalysis, ChemCatChem 12(4) (2019) 1200-1211. DOI: 10.1002/cctc.201901769
[48] T. Butterworth, R. Allen, Plasma-catalyst interaction studied in a single pellet DBD reactor: Dielectric constant effect on plasma dynamics, Plasma Sources Sci. Technol. 26(6) (2017) 065008. DOI: 10.1088/1361-6595/aa6c35
[49] F Peeters, M Sanden, The influence of partial surface discharging on the electrical characterization of DBDs, Plasma Sources Sci. Technol. 24(1) (2014). DOI: 10.1088/0963-0252/24/1/015016
[50] P. Peng, Y. Cheng, R. Hatzenbeller, M. Addy, N. Zhou, C. Schiappacasse, D. Chen, Y. Zhang, E. Anderson, Y. Liu, P. Chen, R. Ruan, Ru-based multifunctional mesoporous catalyst for low-pressure and non-thermal plasma synthesis of ammonia, Int. J. Hydrogen Energy 42(30) (2017) 19056-19066. DOI: 10.1016/j.ijhydene.2017.06.118
[51] A. Ozkan, T. Dufour, A. Bogaerts, F. Reniers, How do the barrier thickness and dielectric material influence the filamentary mode and CO_2 conversion in a flowing DBD?, Plasma Sources Sci.Technol. 25(4) (2016) 045016. DOI: 10.1088/0963-0252/25/4/045016
[52] J. Huang, M. Yuan, X. Li, Y. Wang, Z. You, Inhibited hydrogen poisoning for enhanced activity of promoters-Ru/$Sr_2Ta_2O_7$ nanowires for ammonia synthesis, J. Catal. 389 (2020) 556-565. DOI: 10.1016/j.jcat.2020.06.037
[53] Q. Xie, S. Zhuge, X. Song, M. Lu, F. Yu, R. Ruan, Y. Nie, Non-thermal atmospheric plasma synthesis of ammonia in a DBD reactor packed with various catalysts, J. Phys. D: Appl. Phys. 53(6) (2020) 064002. DOI: 10.1088/1361-6463/ab57e5
[54] P. Mehta, P. Barboun, F.A. Herrera, J. Kim, P. Rumbach, D.B. Go, J.C. Hicks, W.F. Schneider, Overcoming ammonia synthesis scaling relations with plasma-enabled catalysis, Nature Catal. 1(4) (2018) 269-275. DOI: 10.1038/s41929-018-0045-1
[55] J. Shah, T. Wu, J. Lucero, M.A. Carreon, M.L. Carreon, Non-thermal plasma synthesis of ammonia over Ni-MOF-74, ACS Sustainable Chem. Eng. 7(1) (2019) 377-383. DOI: 10.1021/acssuschemeng.8b03705
[56] D. Xie, Y. Sun, T. Zhu, X. Fan, X. Hong, W. Yang, Ammonia synthesis and by-product formation from H_2O, H_2 and N_2 by dielectric barrier discharge combined with an Ru/Al_2O_3 catalyst, RSC Adv. 6 (2016) 105338-105346. DOI: 10.1039/C6RA21351K
[57] Y. Kubota, K. Koga, M. Ohno, T. Hara, Synthesis of ammonia through direct chemical reactions between an atmospheric nitrogen plasma jet and a liquid, Plasma Fusion Res. 5 (2010) 042. DOI: 10.1585/pfr.5.042
[58] M. Bai, Z. Zhang, X. Bai, M. Bai, W. Ning, Plasma synthesis of ammonia with a microgap dielectric barrier discharge at ambient pressure, IEEE Trans. Plasma Sci. 31(6) (2003) 1285-1291. DOI: 10.1109/TPS.2003.818761